Environmental Science Nano

TUTORIAL REVIEW

View Article Online
View Journal | View Issue

Cite this: *Environ. Sci.: Nano*, 2015, **2**, 120

Plasmonic colorimetric and SERS sensors for environmental analysis

Haoran Wei,[abc] Seyyed M. Hossein Abtahi[abc] and Peter J. Vikesland*[abc]

The potential for water pollution outbreaks requires the development of rapid, yet simple detection methods for water quality monitoring. Plasmonic nanostructures such as gold (AuNPs) and silver (AgNPs) nanoparticles are compelling candidates for the development of highly sensitive biosensors due to their unique localized surface plasmon resonances (LSPRs). The LSPR of AuNPs and AgNPs lies in the visible and infrared light range and is sensitive to the composition, size, shape, surrounding medium, and aggregation state of these NPs. This plasmonic behavior provides the basis for fabrication of colorimetric sensors for environmental analyses. Furthermore, the LSPR also enhances the electromagnetic field near the NP surface, which provides the basis for surface-enhanced Raman spectroscopy (SERS) based detection. Organic or inorganic pollutants and pathogens can be detected and differentiated based upon the fingerprint spectra that arise when they enter SERS-active hot spots. In this tutorial review, we summarize progress made towards environmental analysis based on LSPR-based colorimetric and SERS detection. The problems and challenges that have hindered the development of LSPR-based nanosensors for real-world environmental pollutant monitoring are extensively discussed.

Received 22nd December 2014,
Accepted 9th March 2015

DOI: 10.1039/c4en00211c

rsc.li/es-nano

Nano impact

The localized surface plasmon resonance (LSPR) of gold (AuNP) and silver nanoparticles (AgNP) enables rapid identification and detection of environmental pollutants. Using a LSPR-based colorimetric assay it is possible to detect contaminants either visually or *via* spectroscopic approaches. For even greater sensitivity, LSPR enabled surface-enhanced Raman spectroscopy (SERS) makes single molecule or single pathogen detection achievable.

1. Introduction

One notorious side effect of global development is the ever-increasing number of gaseous and aqueous pollutants that pose ecosystem and human-health risks. Rapid pollutant recognition is vitally important in some emergent situations. For example, in the 2014 Elk River, WV incident in excess of 7500 gallons of 4-methylcyclohexanemethanol (4-MCHM) rapidly leaked into the Elk River such that the drinking water distribution system for the greater Charleston, WV area was heavily contaminated.[1] Similarly, in the summer of 2014 a massive algal bloom led to closure of the Toledo, OH drinking water treatment plant due to the contamination of the water by microcystin toxins.[2] In addition to outbreaks caused by chemicals, outbreaks of waterborne pathogens are also problematic. For example, the 1993 Milwaukee *Cryptosporidium* outbreak in drinking water caused 104 deaths in only two weeks.[3] In November 2010, *Cryptosporidium* infected ≈27 000 people in Östersund, Sweden *via* contaminated drinking water, and in December 2012 an outbreak of

[a] *Department of Civil and Environmental Engineering, Virginia Tech, Blacksburg, Virginia, USA. E-mail: pvikes@vt.edu; Tel: (540) 231 3568*
[b] *Virginia Tech Institute of Critical Technology and Applied Science (ICTAS) Sustainable Nanotechnology Center (VTSuN), Blacksburg, Virginia, USA*
[c] *Center for the Environmental Implications of Nanotechnology (CEINT), Duke University, Durham, North Carolina, USA*

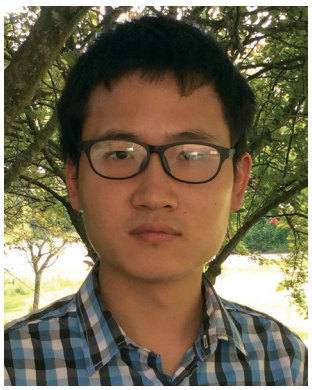

Haoran Wei

Haoran Wei received a MS (July 2013) in Environmental Engineering from Tsinghua University after receiving his BS (June 2010) in Environmental Engineering from Shandong University. He is currently a Ph.D. candidate in Civil and Environmental Engineering at Virginia Tech. His research interests are in the development of nanotechnology-based biosensors for detection of waterborne pathogens or contaminants.

waterborne norovirus caused acute gastrointestinal illness in a district containing 368 families in Denmark.[4,5] In addition to waterborne contaminants, airborne contaminants, such as dioxins from garbage incineration plants or potentially pandemic bird flu, also threaten people's health.[6,7]

To prevent contaminants from causing environmental catastrophes it would be ideal to detect such contamination events as quickly as possible in order to rapidly initiate remedial strategies. Unfortunately, the most commonly used detection methods for water and airborne contaminants such as gas/liquid chromatography-mass spectrometry, inductively coupled plasma mass spectroscopy, and quantitative polymerase chain reaction, although very sensitive and quantitative, require either laborious sample preparation procedures or onerous analysis methods and are thus very time-consuming. Besides, they all require expensive instruments and high level of expertise and thus cannot be conducted on site. Plasmonic nanostructures such as gold and silver nanoparticles (AuNPs and AgNPs) provide a promising avenue for the development of rapid, cost-effective and highly sensitive sensor platforms, which also exhibit the potential for on site detection.[8] Many of the sensing capabilities enabled by AuNPs and AgNPs rely upon localized surface plasmon resonance (LSPR). When excited by light of a specific wavelength, the conduction electrons on the nanoparticle surface collectively oscillate and generate a significantly enhanced electromagnetic field or LSPR.[8–10] LSPR is an extremely sensitive optical transducer, which is dependent on the type, size, shape and aggregation state of plasmonic nanoparticles as well as the refractive index of the surrounding environment.[11–13] Changes in the LSPR result in color changes of the colloid suspension. Based on this phenomenon, LSPR-based colorimetric sensors have been developed.[14–16]

When the incident light wavelength is coupled with the LSPR of plasmonic NPs the electromagnetic field near the NP surface is significantly enhanced.[17,18] When analytes closely associate with the NP surface, their Raman scattering cross-section increases substantially and this phenomenon is the basis for surface-enhanced Raman scattering (SERS).[18] SERS is an ultrasensitive sensing technique that has been shown to enable the detection of single molecules.[19–22] Compared with fluorescent techniques, SERS has greater potential for multiplex analysis due to the narrower peak widths in the collected Raman spectra. Because SERS is a vibrational spectroscopy method it provides chemical bonding information that facilitates differentiation of highly similar molecules and different molecular orientations.[23,24] Unlike other environmental analysis techniques such as inductively coupled plasmon atomic emission spectroscopy and gas chromatography-mass spectroscopy, SERS does not require complex sample pretreatment, sophisticated analytical method optimization, or advanced analyst training. During the last decade, the rapid development of nanotechnology has created a number of novel nanostructures that have the potential for ultrasensitive SERS detection of environmental contaminants.[25–27]

Ultrasensitive chemical analysis *via* SERS was reviewed in the late 1990s, with the focus on the mechanisms responsible for "single molecule detection".[28,29] Subsequently, many review papers have appeared that describe the fundamental theories, material fabrication methods, and applications of SERS.[17,18,21,30–36] Reviews on colorimetric sensors that monitor the LSPR band location have also been produced.[37–39] However, relatively few of these reviews focus explicitly on environmental applications of LSPR based sensing. A number of recent reviews discuss nanomaterial-based sensors for environmental monitoring.[40–45] However, these reviews covered either a broad suite of nanoparticles and sensing

Seyyed M. Hossein Abtahi

Seyyed Mohammad Hossein Abtahi received a second MS (December 2013) in Chemical Engineering from Virginia Tech after receiving his first MS (June 2008) and BS (June 2006) in Chemical Engineering from Sharif University of Technology. He is currently a Ph.D. candidate in Civil and Environmental Engineering at Virginia Tech. His research interests are to assess the colloidal stability, fate, transport, and organismal uptake of anisotropic nanomaterials in aquatic matrices.

Peter J. Vikesland

Peter J. Vikesland is a Professor of Civil and Environmental Engineering at Virginia Tech. He received his BA (1993) in Chemistry from Grinnell College and obtained his MS (1995) and Ph. D. (1998) in Civil and Environmental Engineering from the University of Iowa. After completing a postdoctoral fellowship at Johns Hopkins University he joined the faculty at Virginia Tech in 2002. Vikesland is a NSF CAREER awardee and currently serves as the Co-Director of the Virginia Tech ICTAS Sustainable Nanotechnology Center and the Director of the Virginia Tech Interdisciplinary Graduate Education Program. His research group is interested in the development of nanotechnology-based approaches for the protection of water and air.

techniques or focused exclusively on SERS-based sensors. Herein we focus on the application of AuNPs and AgNPs for environmental sensing *via* either colorimetric or SERS approaches because these two related methods dominate much of the current literature. Readers interested in SPR sensors based on refractive index sensing are referred elsewhere.[46–48] This review is organized into five parts (including this introduction). The second part briefly introduces the photonic behavior responsible for LSPR-based colorimetric and SERS sensors. The third and fourth parts summarize recent progress in environmental analysis with colorimetric and SERS sensors, respectively. In the SERS portion of the review, we focus on organic pollutants, biomolecules, and pathogen detection. For SERS detection of inorganic analytes the reader is referred elsewhere.[49] The concluding part of this tutorial review discusses the extant challenges associated with ultimate application of these sensors in environmental samples.

2. Background on photonics

Colloidal gold and silver nanoparticles exhibit intense colors due to a phenomenon known as surface plasmon resonance.[12,50–52] This phenomenon occurs when conduction band electrons undergo coherent oscillations following excitation by an electromagnetic field. The interaction between the electric field of the incoming light and NPs with dimension smaller than the incident wavelength causes polarization of the electrons in the nanoparticle relative to its heavier ionic core.[53] This net charge difference is confined to the nanoparticle surface and acts as a restoring force that causes the collective oscillation of the surface electrons (*i.e.*, a surface plasmon).[53] The frequency at which these surface plasmons oscillate is known as the LSPR.

The LSPR bands for gold and silver are within the visible portion of the electromagnetic spectrum. For example, the LSPR of spherical 50 nm gold nanoparticles is at ≈530 nm, which falls into the green light range (495–570 nm). Accordingly, green light is absorbed and red light is transmitted thus causing suspensions of this size AuNP to exhibit red colors under visible light excitation. Similarly, the LSPR of spherical 50 nm silver nanoparticles is at ≈430 nm, which falls in the violet light range, leading suspensions of this size AgNP to exhibit green colors.[12,52] The exact location of the LSPR band is highly dependent on the identity, size, shape, and aggregation state of the noble metal nanoparticle, and the chemistry of the suspension medium.[12,50] Increases in size result in red-shifts (an absorption peak shift to a longer wavelength), while changes in shape result in more complicated effects. For example, the peak LSPR wavelength of 100 nm edge-length silver triangles is approximately 100 nm larger than that for 100 nm silver pentagons (pentagon length is defined as the distance between opposite corners), which is in turn 100 nm greater than that of 50 nm diameter silver spheres (Fig. 1).[12] Asymmetric gold nanorods exhibit two LSPR bands – one that corresponds to the longitudinal direction and the other the transverse direction of the rods.[54,55]

In addition to shape mediated effects, changes in aggregation result in quantifiable red-shifts or blue-shifts.[56,57] The potential development of secondary LSPR bands at longer wavelengths has been observed in end-to-end assembly of gold nanorods and at shorter wavelengths in side-by-side assembly of gold nanorods.[56] Although the physics are quite

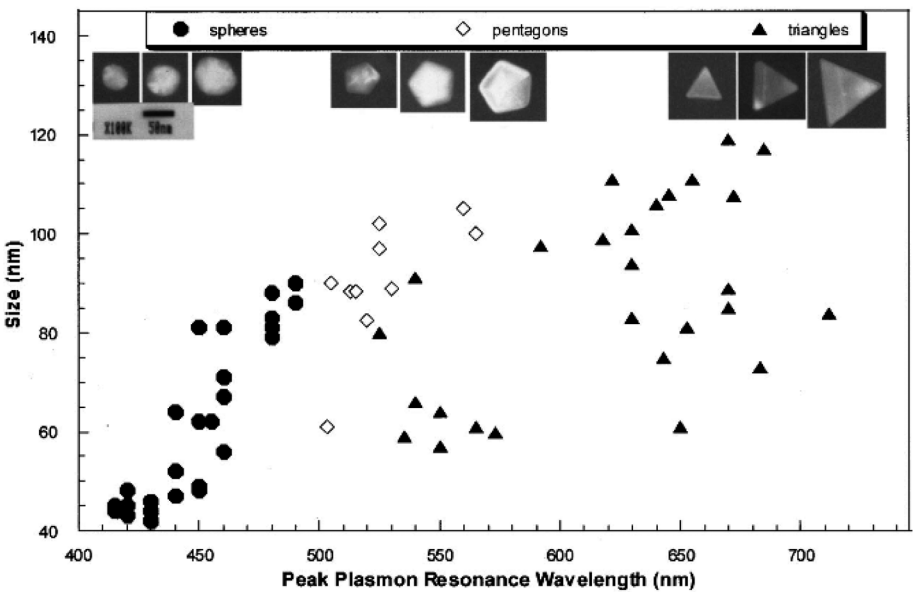

Fig. 1 TEM images of silver spheres, pentagons, and triangles with different size (above) and their size-dependent peak LSPR wavelength. The size of a silver triangle is its edge length; the size of a silver pentagon is the distance between its opposite corners; the size of a silver sphere is its diameter.[12] Reprinted with permission from J. Mock, M. Barbic, D. Smith, D. Schultz and S. Schultz, *J. Chem. Phys.*, 2002, **116**, 6755–6759. Copyright 2014 American Institute of Physics.

complex, in simplistic terms the new LSPR band is the result of dipole alignment between adjacent particles.[58] A tunable LSPR is crucial for sensing applications. The overlap between laser wavelength and the LSPR peak results in high SERS enhancement factors, which will be discussed later.[17] Changes in the LSPR band location can also elicit quantifiable color changes. Using 50 nm AuNPs as an example, aggregation results in the development of a new red-shifted peak at about 700 nm that falls in the red light range. Therefore, red light will be absorbed, while blue light will be scattered and the suspension color changes to blue. Because this color change is distinct and can be easily measured, it has been found to be highly useful for analyte detection.[14,38,59] A broad range of analytes have been detected solely on the basis of this color change.[15,59–61]

Surface-enhanced Raman scattering (SERS) is another phenomenon that arises due to LSPR. A schematic illustrating the basic working principle of SERS is shown in Fig. 2. Raman scattering is the inelastic scattering of photons by the vibrational chemical bonds of a molecule. The Raman spectrum is unique for each molecule due to the different vibrational modes present within it. Unfortunately, the Raman scattering signal is at most 10^{-7} of the total scattering, which makes it challenging to use Raman to detect low concentration analytes. When a molecule is adsorbed on AuNPs or AgNPs, its Raman cross section can be enhanced by several orders of magnitude due to SERS. Two primary mechanisms are responsible for SERS: electromagnetic and chemical. The former refers to the enhanced electromagnetic field near the nanoparticle surface, which is a long-range mechanism.[62] Long-range enhancements occur at greater distances away from the nanoparticle surface whose edge is schematically shown by the dotted red circle in Fig. 2. As shown in Fig. 2, analyte molecules located within the dotted red circle (position 2 and 3) exhibit clear Raman spectra, while analytes located outside the dotted red circle (position 1) exhibit no detectable Raman signal. For example, the SERS signal of the CH_3 group of an alkanethiol molecule decreased by a factor of 2 when its distance from a SERS enhancing silver substrate increased from 0.8 nm to 2.5 nm.[63] The latter reflects charge transfer between the guest molecule and nanoparticle, which is a short-range mechanism.[62] Shorter-range enhancements only occur when an analyte is absorbed to a nanoparticle surface.

Studies to understand the SERS effect have shown that the largest SERS enhancements are produced by strongly interacting metal nanoparticles.[17,64] Clusters of two or more nanoparticles give rise to an extinction spectrum consisting of multiple peaks and facilitate single-molecule SERS.[19] This effect can be attributed to the coupling of the intense localized electromagnetic fields on each nanoparticle produced by incident light excitation of the appropriate wavelength and polarization. The long range coupling of the electromagnetic fields, although it decays exponentially with particle distance, can extend to a distance of 2.5× the nanoparticle diameter.[64,65] It is generally thought that significant Raman enhancements primarily occur within gaps smaller than 10 nm although the exact distance is still a topic of debate.[66–68] These localized areas are often referred to as 'hotspots' (Fig. 2).[69] As shown in Fig. 2, analyte molecules located within the hot spot (position 3) exhibit a much stronger Raman signal than those located on an AuNP monomer surface (position 2). In addition to the gap between two adjacent nanoparticles, the sharp corners and tips of anisotropic plasmonic nanoparticles such as nanorods, nanoprisms, and nanostars produce another type of SERS "hot spot".[70,71] A recent study demonstrated that isolated single gold nanorods can generate strong SERS signals that approach those obtained in the gap between spherical particles.[72] Because of the importance of hot spots for SERS application, a substantial body of research has focused on the creation and maximization of the number and location of SERS hot spots.[73–76]

Other than SERS hot spots, several additional factors significantly influence SERS, such as nanoparticle type, shape, size, solution pH and so on.[77–83] AgNPs can generate stronger SERS intensities than AuNPs because the extinction coefficient of AgNPs can be 4× larger than AuNPs of the same size

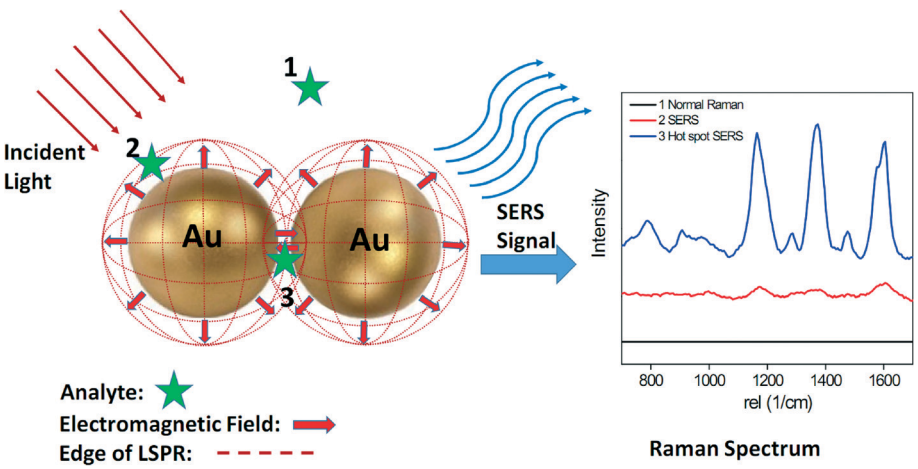

Fig. 2 Schematic of SERS phenomenon for an organic analyte on AuNPs.

and shape.[84,85] Anisotropic plasmonic nanoparticles show multiple LSPR modes and are suitable for use under different laser lines.[86–88] For example, gold nanostars (40 nm) show a second LSPR peak at 730 nm, while gold nanospheres (40 nm) show only one peak at 530 nm. Therefore, when excited by a 785 nm laser, the SERS intensity of gold nanostars is 2–3 orders of magnitude higher than that of gold nanospheres.[89] The size of a nanoparticle affects its LSPR, which determines its SERS intensity as well. A recent study shows even under random aggregation conditions, nanoparticle size still plays an important role in the Raman signal. With 785 nm laser excitation, AuNPs with size between 46–74 nm showed the strongest Raman signal. It has been shown that for elongated shape gold nanoparticles such as rods that the aspect ratio (length/diameter) is an important factor. Results suggest that enhancement can be two orders of magnitude greater when the plasmon band of the gold nanorod overlaps with the excitation wavelength.[90] These results indicate that it is necessary to carefully choose nanoparticle size according to the excitation laser wavelength.[91] Solution pH influences analyte adsorption to the NP surface and can subsequently influence its SERS signal.[77] For example, diclofenac sodium only exhibited a clear SERS spectrum under acidic and neutral pH conditions and not under alkaline pH conditions due to electrostatic repulsion between its carboxylic group and the citrate-coated AgNP surface.[92]

Organic chemical detection is comparatively easy to achieve because small molecules can readily enter SERS hot spots. Pathogens, however, such as bacteria and viruses, are too large to enter SERS hot spots thus resulting in several orders of magnitude lower Raman enhancement factors. To circumvent this problem, a SERS tag is often employed.[31,93] A SERS tag includes a recognition element, Raman reporter, and a signal transducer.[45] AuNPs and AgNPs are most commonly used signal transducers, while dyes with large Raman cross-sections are used as Raman reporters. Specific antibodies or aptamers against the target pathogens are used as recognition elements. Generally, a protection layer is needed for the Raman reporter modified nanoparticle to prevent the leakage of Raman reporter and improve the stability of the nanoparticle.

3. Colorimetric detection

Perhaps the most convenient mechanism for a rapid, field-deployable contaminant detection assay would be to observe color changes with our naked eye. Because the LSPRs of gold and silver colloids fall within the visible spectrum, color changes that occur due to changes in aggregation state have been exploited for colorimetric sensor fabrication. Colorimetric sensing of DNA using functionalized AuNPs was pioneered by Mirkin *et al.*[94] In that study, two batches of 13 nm AuNPs were functionalized with two non-complementary oligonucleotides and were then combined. After the addition of a target DNA duplex with two "sticky ends" (complementary to the oligonucleotides on each type of AuNP), the suspension color changed from red to purple due to DNA hybridization induced AuNP aggregation.[94] Both the oligonucleotide modification position and the AuNP size greatly influenced probe sensitivity. When the two batches of AuNPs were modified with 5′-oligonucleotide and 3′-oligonucleotide, respectively, single base imperfections could be detected.[59] Importantly, larger AuNPs (50 nm, 100 nm) were found to be more sensitive than smaller AuNPs (13 nm) because of their larger extinction coefficients.[95] In addition to oligonucleotide-gold nanoparticle (OGN) conjugates, oligonucleotide-silver nanoparticle (OSN) conjugates were also used as DNA probes. Because of the larger extinction coefficients of AgNPs compared with AuNPs, the detection limit for target DNA by the OSNs was 50× lower than with the OGNs.[96]

Aggregation induced by oligonucleotide hybridization is one example of a cross-linked colorimetric sensor. Similar sensor designs have been applied for detection of a range of biomolecules, heavy metal ions, and pathogens.[97] When the target directly binds to a recognition element on the nanoparticle surface, it induces aggregation and, in the case of AuNPs, a red to blue color change. Alternatively, the target can induce dissociation of nanoparticle aggregates by competitively binding to the linker between nanoparticles. Under these conditions a blue to red color change is expected. For example, an aptamer-linked gold nanoparticle aggregate was developed for adenosine detection. Aptamers are single oligonucleotide strands of DNA or RNA that can bind pathogens, molecules, or even ions with high affinity and specificity.[98] Adenosine addition resulted in dissociation of the aptamer-linked aggregates due to its competitive binding to the aptamer linker between the two AuNPs. Following addition of adenosine, the suspension color changed from purple to red indicating the transformation from AuNP aggregates to monomers. This result was further indicated by the blue shift of the LSPR band in the UV–VIS spectrum from 700 to 522 nm.[99] A similar protocol was successfully applied for the fabrication of a cocaine sensor with a detection limit of 50–500 μM.[61] Recently this protocol was extended to development of a "smart hydrogel" sensor, where dissociation of the cross-linked hydrogel following addition of target resulted in the release of AuNPs to the solution and a change in color.[100]

In a non cross-linked detection protocol there is no hybridization between different gold/silver nanoparticles. In this case, aggregation/dissociation of the nanoparticles is achieved by decreasing/increasing the concentration of stabilizer on the nanoparticle surface. For example, an ultrasensitive colorimetric DNA probe (1 pM detection limit by eye) was developed by using a polyelectrolyte that forms conjugates with single stranded DNA. Following polyelectrolyte addition, AuNPs stabilized with single stranded DNA aggregated due to preferential binding between the aptamer and the polyelectrolyte, while AuNPs stabilized with target double stranded DNA remained stable.[15]

The detection protocols described above have been used for heavy metal detection due to their capacity to form

strong complexes with chelators and other recognition agents. In this manner, a sensitive and selective probe for Hg^{2+} was fabricated by modifying the 13 nm AuNP surface with mercaptopropionic acid (MPA). Hg^{2+} forms complexes with the carboxylate groups of MPA and induces AuNP aggregation. After addition of 2,6-pyridinedicarboxylic acid (PDCA) into the probe suspension, the selectivity for Hg^{2+} relative to other heavy metals was significantly improved. This result was attributed to the 100× higher complexation coefficient of PDCA for Hg^{2+} than for other heavy metals. The combined method enabled quantitative detection of Hg^{2+} over a concentration range of 250–500 nM with a limit of detection of 100 nM.[60] In addition to using toxic organic compounds as recognition elements, urine can also be used for Hg^{2+} sensing. The uric acid and creatinine in urine can synergistically bind to AuNPs as well as selectively adsorb Hg^{2+}. In addition to the low cost sensor fabrication, a low detection limit of 50 nM was achieved in this manner.[16] It has been shown that Zn^{2+} and Cu^{2+} can be detected using agglomeration and the resulting suspension color change of 20 nm chitosan-capped gold nanoparticles.[101] Chitosan is a well-known chelating agent for heavy metals and the presence of Zn^{2+} and Cu^{2+} can cause colloidal instability and loose aggregation (agglomeration) of gold nanoparticles. This phenomenon causes a rapid color change that is directly related to the heavy metal concentration. Pb^{2+} with a tunable detection limit of 100 nM to 200 μM has been detected following an aggregation-dissociation protocol. The DNAzyme-directed assembly of gold nanoparticles cleaves in the presence of Pb^{2+} and results in a blue to red color change (Fig. 3A).

Nitrate and nitrite ions are two regulated contaminants in drinking water. A simple colorimetric method was developed for their detection based upon the Griess reaction (Fig. 3B). As shown in Fig. 3B, two batches of AuNPs were functionalized with 5-[1,2]dithiolan-3-yl-pentazoic acid [2-(4-aminophenyl)ethyl]amide (DPAA) and 5-[1,2]dithiolan-3-yl-pentazoic acid [2-(naphthalene-1-ylamino)ethyl]amide, respectively. Following nitrite ion addition, the amino group and naphthalene group were linked *via* an azide linkage, which then resulted in AuNP aggregation and the fading of the suspension color. The color change threshold could be controlled by adjusting the incubation time and temperature to meet the EPA standard (1 ppm for nitrite ion). The same procedure was applied for nitrate detection after the nitrate ions were reduced to nitrite by nitrate reductase. The specificity of this probe is high enough that it is not affected by the presence of other inorganic ions (F^-, SO_4^{2-}, HCO_3^-, *etc.*) even when

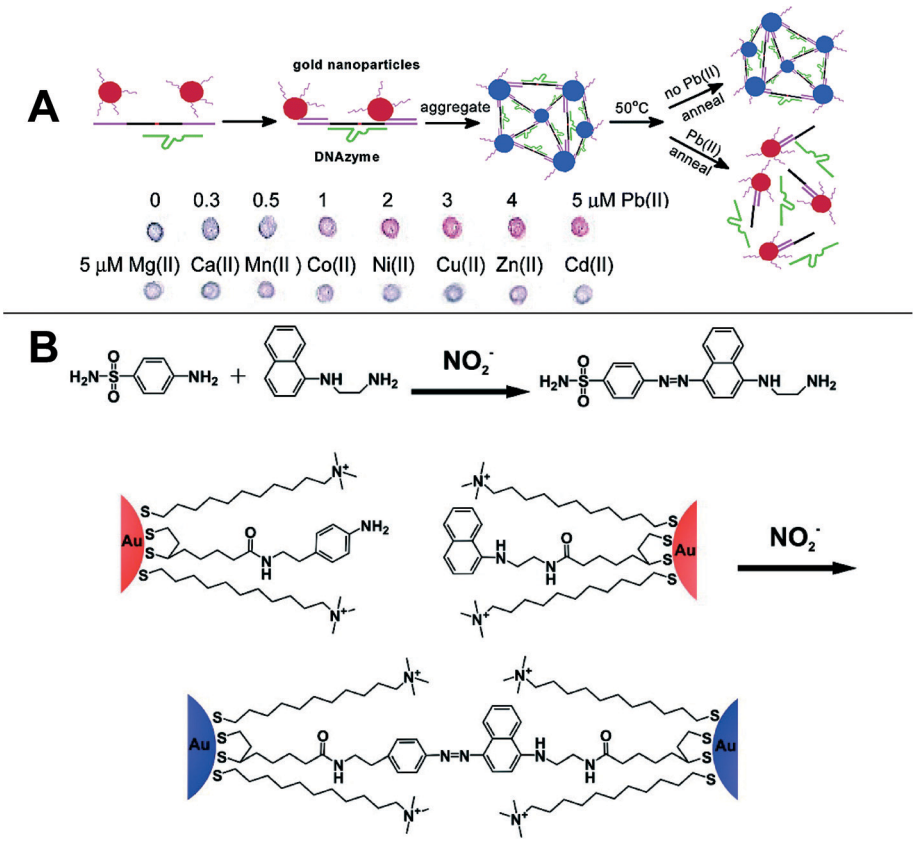

Fig. 3 A) DNAzyme-directed assembly formation and cleavage of gold nanoparticles in a Pb^+ colorimetric sensor;[102] Reprinted with permission from J. Liu and Y. Lu, *J. Am. Chem. Soc.*, 2003, **125**, 6642–6643. Copyright 2014 American Chemical Society. B) Schematic of the Griess reaction and Griess reaction induced aggregation of AuNPs.[14] Reprinted with permission from W. L. Daniel, M. S. Han, J. S. Lee and C. A. Mirkin, *J. Am. Chem. Soc.*, 2009, **131**, 6362–6363. Copyright 2014 American Chemical Society.

their concentrations are two orders of magnitude larger than that of nitrite.[14]

A majority of the plasmonic nanoparticle based colorimetric detection methods rely upon crosslinking. However, non-crosslinking methods are also sometimes employed. A homogeneous method for the selective detection of Hg^{2+} and Ag^{+} using Tween 20-modified AuNPs has been developed. Citrate-capped AuNPs were modified with Tween 20. In the presence of silver and mercury ions, citrate ions reduce Hg^{2+} and Ag^{+} to form Hg^{0} and Ag^{0} on the surface of the AuNPs. This phenomenon was followed by Tween 20 removal from the NP surface and aggregation of AuNPs. The detection limit can be as low as 0.1 μM in the presence of NaCl and EDTA.[103] In another study, a sensor for quantitative detection and differentiation of two nitroamine explosives – hexahydro-1,3,5-trinitro-1,3,5-triazine (RDX) and octahydro-1,3,5,7-tetranitro-1,3,5,7-tetrazocine (HMX) was developed.[104] In this sensor, nitrite hydrolyzed from RDX and HMX reacted with 4-aminothiolphenol on AuNPs to form an azo dye with naphthylene diamine. Dye formation changed the LSPR of the AuNPs because of a charge-transfer interaction on the AuNP surface. The absence of a second LSPR peak indicated the color change was not due to AuNP aggregation, but instead due to dye formation. AuNPs improved the sensitivity of the probe, but the mechanism responsible for this behavior was not clearly elucidated.

Some special detection protocols have also been used for heavy metal ion detection. Cr^{6+} can selectively etch the tips of gold nanorods (AuNRs) due to its strong oxidation state. Shortening of the nanorod induces a blue shift in its longitudinal LSPR band and a corresponding color change. Using this approach a detection limit of 90 nM was obtained.[105] This method does not require aggregation or dissociation of nanoparticles and as such it can be described as a non-aggregation method. Cu^{2+} can also etch the tips of AuNRs in the presence of HBr. In this case, Au^{0} was oxidized to Au^{+} and Cu^{2+} was reduced to Cu^{+}, which was subsequently oxidized to Cu^{2+} by dissolved oxygen (Fig. 4A). The presence of cetyltrimethylammonium bromide (CTAB) was key to this redox reaction because it reduced the redox potential of Au^{+}/Au^{0} from 0.93 V to less than 0.2 V. The decrease in aspect ratio due to etching resulted in a blue shift of the LSPR band and a color change from blue to red (Fig. 4A). With this method, 50 nM Cu^{2+} was detected by the naked eye and 0.5 nM Cu^{2+} was detectable by UV–VIS.[106] A similar protocol was applied for Hg^{2+} detection. In the presence of ascorbic acid,

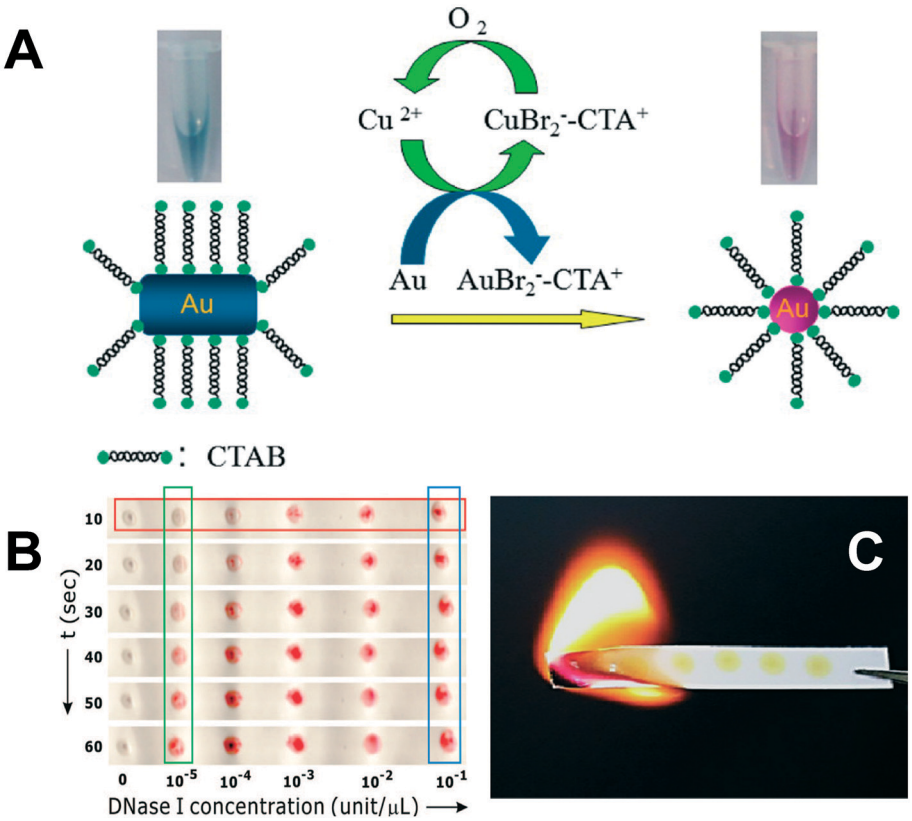

Fig. 4 A) Schematic of colorimetric detection of Cu^{2+} by etching AuNR tips by Cu^{2+} in the presence of CTAB and HBr.[106] Reprinted with permission from Z. Zhang, Z. Chen, C. Qu and L. Chen, *Langmuir*, 2014, **30**, 3625–3630. Copyright 2014 American Chemical Society. B) DNA-hybridized AuNP aggregates on a hydrophobic paper after exposure to DNase I droplets.[108] Reprinted with permission from W. Zhao, M. M. Ali, S. D. Aguirre, M. A. Brook and Y. Li, *Anal. Chem.*, 2008, **80**, 8431–8437. Copyright 2014 American Chemical Society. C) Spent paper substrates are burnt to minimize hazardous chemical handling.[109] Reprinted with permission from S. C. Tseng, C. C. Yu, D. Wan, H. L. Chen, L. A. Wang, M. C. Wu, W. F. Su, H. C. Han and L. C. Chen, *Anal. Chem.*, 2012, **84**, 5140–5145. Copyright 2014 American Chemical Society.

Hg^{2+} was reduced to Hg^0 and deposited on AuNRs, which induced a color change from purple to blue green. The detection limit of Hg^{2+} was 800 pM. The Hg^0–AuNR can subsequently be used as a S^{2-} sensor because S^{2-} can exfoliate Hg^0 from the AuNR surface.[107]

For practical field applications, paper-based colorimetric sensors may be better than suspension-based ones due to their smaller volume, longer-term stability, and convenient handling and processing. Recently it has been reported that the protocols for suspension-based colorimetric detection can also be applied on a paper substrate.[108,110] For example, DNA-hybridized AuNP aggregates that were spotted on paper can be redispersed into a droplet that contains endonuclease (DNase I), which could cleave hybridized DNA. Following endonuclease addition, the blue or black spot on paper rapidly changed color to red and this color change could be discerned by the naked eye even at low nM endonuclease concentrations (Fig. 4B).[108] It is notable that the paper used in these assays should be hydrophobic paper or surfactant-treated hydrophilic paper to avoid the rapid spread and drying of the droplet applied on the surface. In addition to drop-coated AuNP suspensions on paper, paper/AuNP composites can also be synthesized by a laser-induced thermal method. When 15 nm thin gold films coated on paper were exposed to KrF excimer laser irradiation, AuNPs (46 nm) formed on the paper surface with a high density of 318 μm^{-2}. Following immersion into cysteine solution the color of the paper changed from light yellow to dark yellow. The paper could be burnt after use, which is a simple mechanism for hazardous waste disposal (Fig. 4C).[109] Another paper-based analytical protocol has been reported for colorimetric sensing of Cu^{2+} by AgNPs functionalized with homocysteine and dithiothreitol. The LSPR peak intensity of AgNPs at 404 nm decreased while a new red-shifted band at 502 nm appeared as Cu^{2+} was added. Consequently, the color of the paper coated with AgNPs changed from yellow to orange or green-brown. A linear response was observed for the color intensity change as a function of Cu^{2+} concentration in the range of 7.8–62.8 μM.[111] Based on these results, we are confident that paper-based colorimetric LSPR sensors should have applicability for detection of a broad range of environmental pollutants.

4. SERS detection

The SERS phenomenon was first observed in 1974 when the Raman signal of pyridine adsorbed on a roughened silver electrode was substantially enhanced.[112] SERS was subsequently proposed as an analytical technique for many organic compounds using substrates such as roughed Ag electrodes or Ag films on nanospheres (AgFON).[113,114] However, the detection limits achieved with these methods are high (above 1 μM), which limits their application. In 1997, however, single molecule detection was achieved for resonant dye molecules, such as rhodamine 6G (R6G) and crystal violet (CV) using AgNP colloids as SERS substrates.[19,22] It was subsequently realized that aggregates in the colloid are responsible for the substantially enhanced Raman signal and the concept of the aforementioned SERS "hot spot", the gap between the aggregates, was proposed.

In the past decade, numerous research efforts have been devoted to create and maximize the number of "hot spots" within SERS substrates.[116,118,119] Adding salts or organic electrolytes to gold or silver colloid suspensions can induce aggregation and generate SERS "hot spots".[120] However, the aggregation process is random and thus hard to replicate. Recently, methods to generate highly reproducible and controllable SERS hot spots in suspension have been reported.[115,116,121,122] For example, the supermolecule cucurbit[*n*]uril (CB[*n*]) can link AuNPs with a fixed gap of 0.9 nm and this molecule can also specifically capture target analytes within the hot spot (Fig. 5A).[115] DNA-mediated gold nanogap particles, which contain a 20 nm gold core and 11 nm gold shell linked by a gold nanobridge have recently been synthesized (Fig. 5B). Dyes located in the 1 nm gap were quantitatively detected over an ultra low concentration range of 10 fM to 1 pM. Raman mapping results demonstrate that 90% of these nanoparticles show SERS enhancement factors between 10^8 and 10^9 – a range that is sufficient for single molecule detection.[116] Despite its excellent homogeneity, this nanoparticle is more appropriate for use as a SERS tag rather than as a SERS substrate due to the difficulty associated with getting analyte chemicals to diffuse into the nanogap.

For real applications, solid SERS substrates are often considered superior to suspension-based SERS due to the long term stability and transport and handling convenience that the solid substrates provide. Extensive research efforts have been devoted to making homogeneous solid SERS substrates using approaches such as electron lithography, focused ion beam lithography, and nanosphere lithography.[13,20,33,82,123–125] These top-down methods make highly ordered plasmonic nanostructures with tunable shape, size, and particle-to-particle gap size and have very high SERS enhancement factors.[126] However, these methods, especially electron lithography, can be quite expensive and are difficult to scale up. Recently reported nanoporous gold and gold/silver nanoporous films are easy to make at large scale. After thermal treatment, the films wrinkle and create quasi-periodic nanogaps and nanotips, which act as SERS "hot spots". With these wrinkled films, single molecule detection of R6G was achieved.[20,123] Recent studies find that covering Au nanopyramid arrays with graphene can improve the SERS signal 10× due to the enhanced charge transfer.[127]

In contrast to the aforementioned rigid SERS substrates, flexible substrates such as paper-based SERS substrates are cheaper, easier to make, and can be applied for curvy surfaces.[128–134] A paper-based SERS swab was fabricated by simply dipping a filter paper in AuNR suspension. AuNRs were adsorbed efficiently onto the surface of filter paper due to the electrostatic attraction between the negatively charged cellulose and the positively charged CTAB-coated AuNRs. The

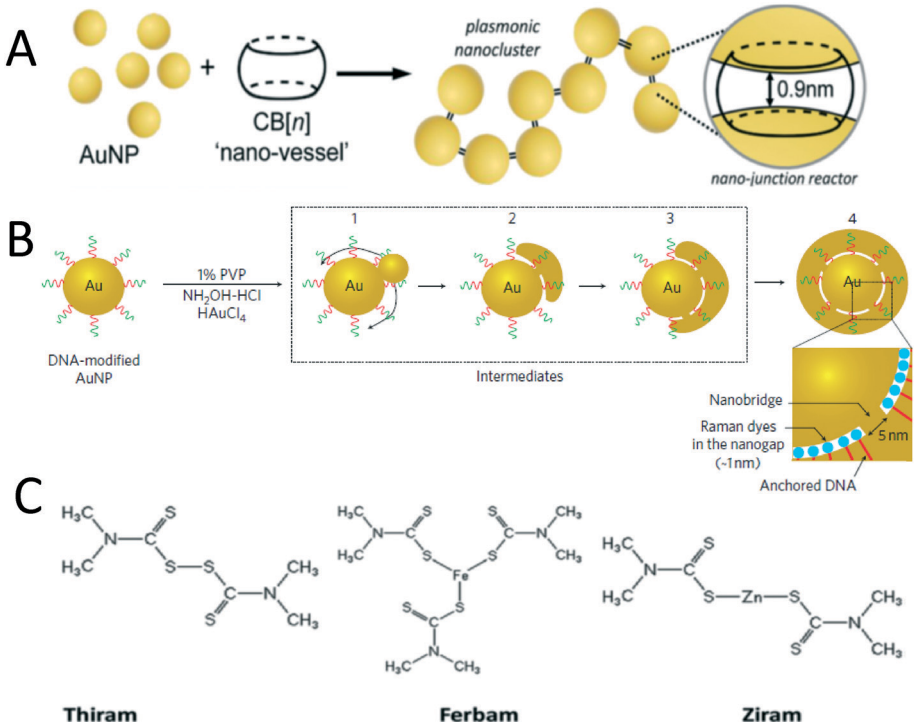

Fig. 5 A) CN[*n*] induced AuNP aggregation with a fixed sub nanometer gap;[115] Reprinted with permission from R. W. Taylor, R. J. Coulston, F. Biedermann, S. Mahajan, J. J. Baumberg and O. A. Scherman, *Nano Lett.*, 2013, **13**, 5985–5990. Copyright 2014 American Chemical Society. B) Formation of 1 nm gap between AuNP core and shell linked with a Au nanobridge.[116] Reprinted with permission from D. K. Lim, K. S. Jeon, J. H. Hwang, H. Kim, S. Kwon, Y. D. Suh and J. M. Nam, *Nat. Nanotechnol.*, 2011, **6**, 452–460. Copyright 2014 Nature Publishing Group. C) Chemical structures of three dithiolcarbamate pesticides.[117] Reproduced from B. Saute, R. Premasiri, L. Ziegler and R. Narayanan, *Analyst*, 2012, **137**, 5082–5087. With permission from The Royal Society of Chemistry. Copyright 2014 The Royal Society of Chemistry.

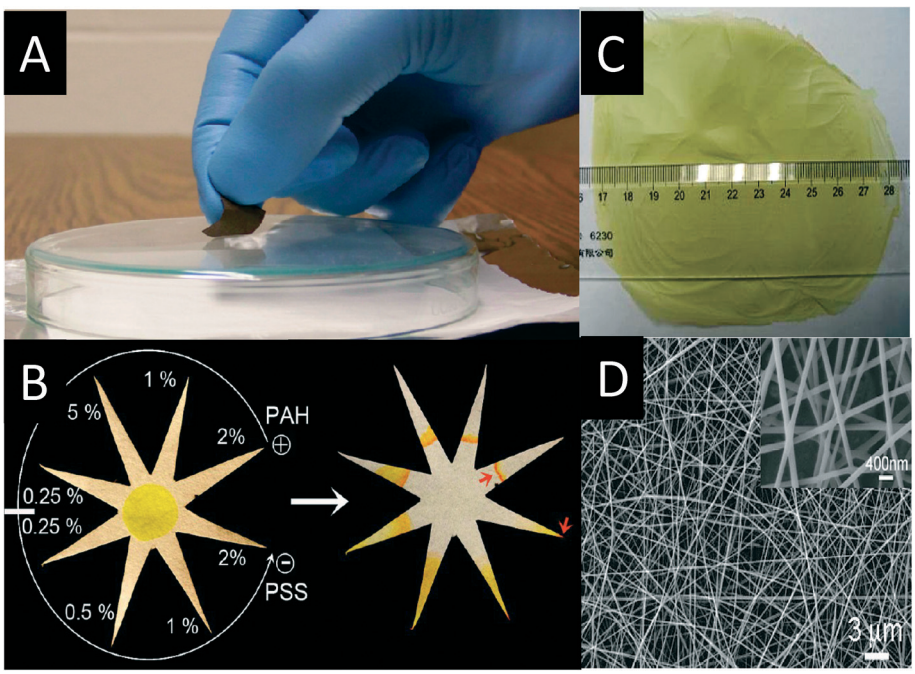

Fig. 6 A) A glass with 1,4-BDT residue is swabbed by the paper-based SERS substrate;[129] Reprinted with permission from C. H. Lee, L. Tian and S. Singamaneni, *ACS Appl. Mater. Interfaces*, 2010, **2**, 3429–3435. Copyright 2014 American Chemical Society. B) A star-shape paper with eight fingers were coated by polyelectrolyte, which could separate and preconcentrate chemicals efficiently;[133] Reprinted with permission from A. Abbas, A. Brimer, J. M. Slocik, L. Tian, R. R. Naik and S. Singamaneni, *Anal. Chem.*, 2013, **85**, 3977–3983. Copyright 2014 American Chemical Society. C) The photo and D) SEM image of AgNP/PVA membrane fabricated by electrospinning.[135] Reprinted with permission from D. He, B. Hu, Q. F. Yao, K. Wang and S. H. Yu, *ACS Nano*, 2009, **3**, 3993–4002. Copyright 2014 American Chemical Society.

biggest advantage of this SERS substrate is its ease of use for the collection of trace samples from a solid surface. By swabbing a glass surface contaminated with a 140 pg 1,4-benzenedithiol (1,4-BDT) residue, the chemicals were readily adsorbed on the paper surface and their Raman spectrum was easily obtained (Fig. 6A).[129] Similarly, a star-shaped μPAD whose fingers were coated with polyelectrolyte was fabricated (Fig. 6B). This μPAD showed the capability to separate chemicals based upon their charge and to concentrate the chemicals into the small volume of the tips (Fig. 6B). For example, positively charged R6G readily moved to the finger tip coated with positively charged poly(allylamine hydrochloride), while it was retained at the entrance of the finger coated with negatively charged poly(sodium 4-styrenesulfonate). This μPAD exhibited a preconcentration factor of 10^9 for R6G and thus a super low detection limit of 100 aM was detected.[133] In addition to paper, electrospun nanofiber mats have also been used as the SERS substrate scaffold.[134,135] For example, an AgNP/PVA (poly(vinyl alcohol)) membrane was fabricated by electrospinning AgNPs and PVA mixture. The bulk material and nanofibers coated with AgNPs are shown in Fig. 6C and D, respectively. 4-mercaptobenzoic acid (4-MBA) at a concentration of 10^{-6} M was detected using this SERS substrate.[135]

Although significantly improved average enhancement factors (EF) have been achieved (generally greater than 10^9) for Raman active dyes and other test materials, the application of such SERS substrates for ultrasensitive detection of organic pollutants are few.[117,136–140] The reason for this is that many organic pollutants are non-resonant under the laser excitation wavelengths (>514 nm) typically used for Raman spectroscopy. Accordingly, their Raman cross-sections are generally several orders of magnitude lower than those for the resonant dyes most commonly used for SERS substrate development.

SERS detection of pesticides with high affinity to AuNPs has been reported.[117,138] Dithiolcarbamate pesticides – thiram, ferbam, and ziram were detected and differentiated by SERS using a gold nanorod suspension as the SERS substrate. The structures of these three chemically similar pesticides are shown in Fig. 5C. Each pesticide contains sulfur groups that can form covalent Au–S bonds with the AuNP surface. To obtain high SERS intensity, gold nanorods whose longitudinal LSPR was well coupled with the laser wavelength were used as the SERS substrate. The detection limits of these three pesticides are 34 nM, 26 nM, and 13 nM, respectively, well below the EPA standards (17 μM, 10 μM, 23 μM).[117] These results indicate that for organic pollutants showing high affinity with gold or silver nanoparticles, SERS detection is feasible if the LSPR of the SERS substrate matches the excitation laser wavelength. An organophosphorus pesticide – paraoxon at a concentration of 10 nM was detected using a self-assembled gold nanoparticle film. The film is made by casting methoxy-mercapto-poly(ethylene glycol) (mPEG-SH) functionalized AuNP suspension onto a solid substrate. The AuNPs were closely packed on the substrate with 5 nm gaps. Self-assembly induced by mPEG-SH modification significantly improved the SERS intensity and homogeneity of the film.[138] This is a simple and cost-efficient method for SERS substrate fabrication. However, the author did not explain how the mPEG-SH-AuNP suspension and the analyte solution overcame the "coffee ring effect" when cast on a solid substrate.

A significant challenge that has limited SERS detection of organic pollutants is not only their generally small Raman cross sections, but also their low affinity to the NP surface. Therefore, methods to enhance the affinity between pollutants and the gold/silver NP surface have been pursued to solve this problem.[141–146] One way to achieve this goal is through addition of a molecular trap on the gold/silver nanoparticle surface to specifically capture organic molecules. The thermally sensitive polymer poly-(*N*-isopropylacrylamide) (pNIPAM) was recently used as the trap for 1-naphthol (1-NOH). At a temperature of 277 K, pNIPAM exists in a swollen state, such that 1-NOH trapped within the polymer is far away from the AuNP surface, which then results in a weak SERS signal. In contrast, at a temperature of 333 K, pNIPAM shrinks to half of its swollen volume, thus bringing 1-NOH closer to the AuNP surface resulting in a substantial increase in the SERS signal.[143] This method enabled acquisition of the SERS spectrum of 1-NOH for the first time. However, the limit of detection for 1-NOH is high (10 μM). TNT was trapped on a cysteine-functionalized AuNP surface by the formation of a Meisenheimer complex with cysteine (Fig. 7A). Electrostatic attraction between Meisenheimer complex-bound AuNPs and cysteine-bound AuNPs subsequently resulted in AuNP aggregation and the generation of a number of SERS hot spots. With this method, 2 pM TNT was detected in aqueous solution.[141] TNT has also been adsorbed onto the AuNR surface by a peptide linker containing a TNT-binding tail, a cysteine terminal, and a glycine spacer. The peptide-functionalized AuNRs were embedded in a filter paper and tested with both liquid phase and vapor phase TNT. Notably, this material could detect 10 μM TNT in a shampoo solution thus indicating its high selectivity for TNT.[147] Dithiolcarbamate calix[4]arene was also used as a linker between AgNPs and polycyclic aromatic hydrocarbons (PAHs). The cup shape calix[4]arene is able to host hydrophobic PAHs and the dithiolcarbamate on the linker increases the affinity between the linker and the nanoparticle (Fig. 7B). This novel SERS substrate can achieve a limit of detection for four PAHs (pyrene, benzo[*c*]phenanthrene, triphenylene, and coronene) in the range between 10 nM to 100 pM.[142] Calixarene-functionalized AgNP embedded in silica film was applied in a flow cell designed for *in situ* monitoring of PAHs in seawater.[148–150] Limits of detection of 100 pM and 310 pM for pyrene and anthracene were achieved when artificial sea water spiked with PAHs traveled through the flow cell.[148] A field study using this SERS substrate was conducted in the Gulf of Gdańsk (Baltic Sea). The limit of detection for 12 different PAHs was 150 ng L^{-1}, which is comparable to the results obtained *via* GC/MS, thus indicating the SERS technique has potential for monitoring pollution events *in situ*.[150]

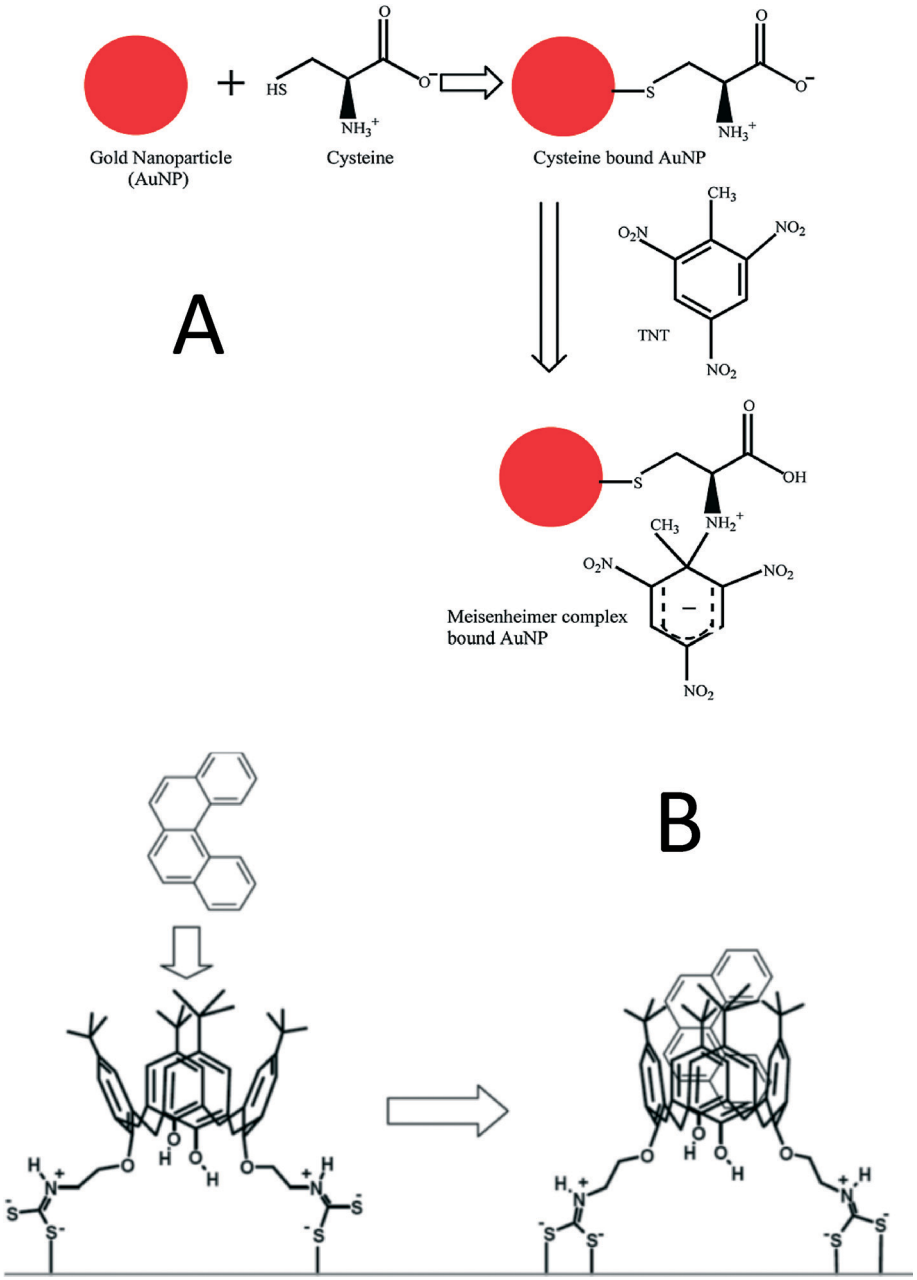

Fig. 7 A) Trinitrotoluene (TNT) is captured by cysteine-functionalized AuNPs by formation of a Meisenheimer complex;[141] Reprinted with permission from S. S. Dasary, A. K. Singh, D. Senapati, H. Yu and P. C. Ray, *J. Am. Chem. Soc.*, 2009, **131**, 13806–13812. Copyright 2014 American Chemical Society. B) calix[4]arene links PAHs and AgNPs.[142] L. Guerrini, J. V. Garcia-Ramos, C. Domingo and S. Sanchez-Cortes, *Anal. Chem.*, 2009, **81**, 953–960. Copyright 2014 American Chemical Society.

Viologens have also been used as a PAH linker. Because of their high affinity to both AgNPs and guest PAHs, viologens could induce the aggregation of AgNPs and thus further increase the SERS intensity. With this method, a detection limit of 80 pyrene molecules was obtained – this is the lowest limit of detection for pyrene ever reported.[144] The drawback of this method is the high background signal from the linker, which makes spectrum analysis challenging.

The SERS spectrum of the dioxin 2-benzoyldibenzo-*p*-dioxin (BDPD), a highly toxic compound, was first reported in 2009 using AgNPs loaded in poly(diallyldimethylammonium chloride) (PDDA) and poly-(acrylic acid) (PAA) film. This film was fabricated using a layer-by-layer method and subsequently impregnated with AgNPs. After drying in air, this SERS substrate showed a 5× higher Raman signal for 1-naphthalenethiol (1-NAT) than an AgNP suspension due to hot spot formation in the 3D structure. More importantly, the SERS dioxin spectrum at 10 nM was observed on this substrate although the signal was very weak.[140] This substrate works for dioxin partly because the PDDA–PAA can trap

dioxin in the film thus creating the opportunity for dioxin contact with the AgNP surface. Recently, a detection limit down to three molecules was reported for atrazine detection *via* SERS.[151] This detection limit was achieved by directly adding a specific volume of 100 μM atrazine to an AgNP colloid suspension. This result demonstrates that SERS achieved similar detection limit (ppt) to sophisticated liquid chromatography-tandem mass spectroscopy (LC-MS/MS) and outperformed it due to its facile operation and fast measurement. However, this paper did not report a detailed characterization of the SERS substrate, the Raman measurement conditions, or the reproducibility of the data. The reason why the authors were able to achieve such a low detection limit is probably the addition of high concentrations of atrazine (100 μM) that induced AgNP aggregation. More research efforts are required in this field to discuss if SERS can be used for single or few molecule detection of organic pollutants in environmentally relevant samples.

To facilitate on site pollutant detection, a portable Raman instrument integrating a SERS sensor is highly desired.[152,153] Recently such an instrument containing a silver dendrite SERS substrate was developed for pesticide detection. The large laser spot of 2 mm minimizes SERS intensity variation among parallel samples. The pesticide ferbam with concentrations of 0 ppm, 4 ppm, 7 ppm, and 14 ppm was used as reference materials indicating no risk, low risk, risk, and high risk, respectively. The self checking tests for the four references all passed, indicating this instrument shows potential for on site pesticide detection.[152] Combining microfluidic chips and SERS substrates in the portable Raman instrument is promising for real-time on site pollutant detection. With a micropillar array PDMS chip integrated in the instrument, complete mixing of the two confluents – AgNPs and pollutants (dipicolinic acid and malachite green) is achieved. Dipicolinic acid and malachite green were quantitatively detected with limits of detection of 200 ppb and 500 ppb, respectively.[153]

For larger targets, such as biomolecules, viruses, cancer cells, bacteria and protozoa, it is very difficult to directly acquire their SERS spectra by adding them to SERS substrates because they are too big to fit into the hot spots due to their large size.[155,156] Instead, a SERS tag is used to specifically bind the targets and the SERS spectrum of a Raman reporter functionalized on the SERS tag is then monitored.[93,157] Raman reporter is usually a dye having a large Raman cross section. Ideal SERS tags are able to generate strong enough signals for single target detection. Interested readers are referred to a very good review for additional details on SERS tags.[31] Yang *et al.* fabricated a nanopillar-based SERS substrate to detect the macromolecule vasopressin, which was labeled by a Raman reporter 5-carboxytetramethylrhodamine. The nanopillar is made by depositing gold vapor onto etched silicon wafer. The coated gold film on the tip of silicon wire formed a pillar, which was functionalized with a vasopressin-specific aptamer. After exposure to vasopressin and subsequent drying, the intensified SERS signal of TAMRA was acquired due to the capillary force-driven aggregation of the nanopillars. The detection limit of vasopressin was reported to be 1 pM.[119] Recently, graphene oxide (GO) was used for SERS tag fabrication because of its capacity to significantly enhance the SERS signal.[154,158] The schematic of this SERS tag synthesis is shown in Fig. 8. Different from the traditional SERS tag fabrication, the Raman reporter – tris(2,2′-bipyridyl)ruthenium(II) chloride (Rubpy) was first adsorbed

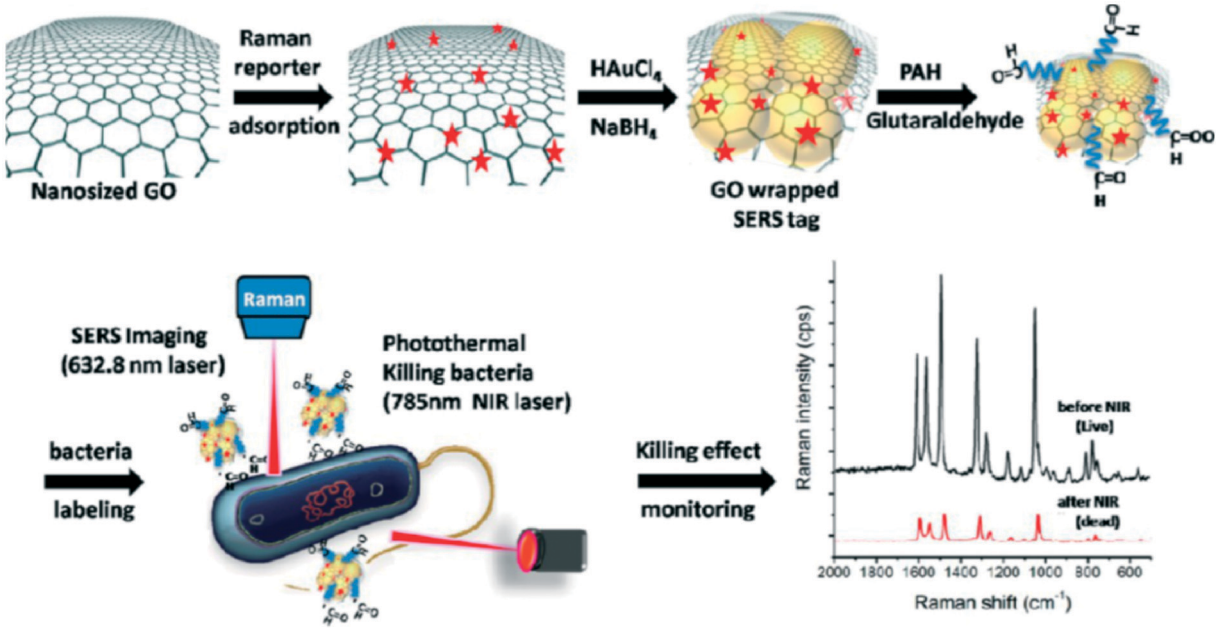

Fig. 8 Schematic for AuNP/GO/Rubpy/GA SERS tag synthesis and its application for monitoring the photothermal ablation of bacteria.[154] Reprinted with permission from D. Lin, T. Qin, Y. Wang, X. Sun and L. Chen, *ACS Appl. Mater. Interfaces*, 2014, **6**, 1320–1329. Copyright 2014 American Chemical Society.

on GO and subsequently AuNPs formed by *in situ* reduction of $HAuCl_4$ on GO/Rubpy. GO was able to not only enhance the SERS signal by two fold but also improve the colloid stability by wrapping around the small nanoparticle aggregates. AuNP/GO/Rubpy was subsequently functionalized with positively charged poly(allylamine hydrochloride) (PAH), which provided amine groups to link to the recognition element glutaraldehyde (GA). GA can bind to both gram-positive and gram-negative bacteria by crosslinking with the peptidoglycan layer on their surfaces. In addition to its single cell identification capability, this SERS tag can also be used for photothermal ablation of bacteria when exposed to a 400 mW 785 nm laser. The decrease in the SERS signal can be used to monitor the bacterial ablation process (Fig. 8).[154]

Although detecting large targets using SERS tags can achieve very high sensitivity, it is complex and costly to fabricate these tags. Most recently, the SERS spectrum of virus on SERS substrates without a SERS tag has been reported. This is called label-free SERS detection of virus.[159] Progress made in this promising area of research was recently summarized elsewhere.[159] Briefly, a highly sensitive and reproducible SERS substrate was fabricated by oblique angle deposition. The obtained SERS substrate contains tilted silver nanowire arrays. Virus was directly added to the SERS substrate and its SERS spectrum was readily acquired. Using this technique, three viruses – adenovirus, rhinovirus, and HIV were distinguished and even different strains of respiratory syncytial virus (RSV) could be differentiated. This approach was also applied to measure the SERS spectrum of RSV in its infected cell lysate although the background interference is strong. These results indicate that label-free detection of virus is feasible if SERS substrates are well designed. However, the weak signal, strong background disturbance, and subtle change of spectrum between different viruses make the data analysis challenging. Principle component analysis (PCA) and other chemometic approaches are often required to differentiate the viruses from the background and from one another.

5. Challenges

Although the rapid development of nanotechnology has facilitated substantial progress towards improved colorimetric and SERS detection, the high costs of sensor fabrication still impede their practical environmental applications. Development of low-cost and scalable detection platforms remains a big challenge. It is thus desirable to incorporate detection components within paper or other sustainable materials without using costly lithography techniques. Paper-based colorimetric sensors can be used at home to monitor drinking water quality by simply dipping test strips into water. However, the sensitivity and resistance of these test strips to potential interferents such as drinking water disinfectants should be improved to make such a sensor truly useful. SERS sensors have the capacity to replace the complex lab assays currently used in water and wastewater treatment plants because of their simple sample preparation and rapid detection process. Suspension-based sensors may not be appropriate for use in real water samples since the colloids may not be stable in complex water chemistries and the challenges associated with long-term storage. As noted, paper-based SERS substrates have potential application. However, their SERS hot spot densities and affinities for specific organic pollutants currently do not meet real world application requirements. It is a considerable challenge to develop universal SERS substrates that have broad applicability to all of the organic chemicals of interest because the size, polarity, and isoelectric point of the chemicals determine their capacity to enter the hot spots on the SERS substrate. For on-site detection, portable SERS instrumentation is required and those systems currently rely only on near infrared lasers because of their ease of miniaturization. Accordingly, the SERS substrate must be optimized for application with near infrared lasers. Unfortunately, most organic pollutants are non-resonant at this laser wavelength, which makes their detection more challenging. Moreover, if we want to achieve real-time detection, the laser integration time must be very short, which further increases the difficulty. In addition to organic pollutant detection, SERS sensors also show potential for label-free pathogen detection. Since pathogens are generally too large to readily enter hot spots, the SERS substrate must have extremely high enhancement factor to make the pathogen spectrum visible. The reproducibility of SERS pathogen detection is also challenged because the contact between pathogens and Au or AgNPs may vary with time. The steps required for development of low-cost and efficient SERS substrates for pathogen detection are an ongoing area of research focus.

Acknowledgements

Funding for this study was provided by the US National Science Foundation (NSF; CBET 1236005 and 1133736) and the Virginia Tech Institute for Critical Technology and Applied Science. Support for HW was provided by the Virginia Tech Graduate School through the Sustainable Nanotechnology Interdisciplinary Graduate Education Program (VTSuN IGEP). Additional funding was provided by NSF and the Environmental Protection Agency under NSF Cooperative Agreement EF-0830093, Center for the Environmental Implications of NanoTechnology (CEINT). Any opinions, findings, conclusions or recommendations expressed in this material are those of the authors and do not necessarily reflect the views of the NSF or the EPA. This work has not been subjected to EPA review and no official endorsement should be inferred.

References

1 J. Manuel, *Environ. Health Perspect.*, 2014, **122**, A214–A219.
2 C. Fitzpatrick, *Water21 - Magazine of The International Water Association*, 2014.
3 W. R. Mac Kenzie, N. J. Hoxie, M. E. Proctor, M. S. Gradus, K. A. Blair, D. E. Peterson, J. J. Kazmierczak, D. G. Addiss,

K. R. Fox and J. B. Rose, *N. Engl. J. Med.*, 1994, **331**, 161–167.
4 M. Widerström, C. Schönning, M. Lilja, M. Lebbad, T. Ljung, G. Allestam, M. Ferm, B. Björkholm, A. Hansen and J. Hiltula, *Emerging Infect. Dis.*, 2014, **20**, 581–589.
5 L. B. van Alphen, F. Dorléans, A. C. Schultz, J. Fonager, S. Ethelberg, C. Dalgaard, M. Adelhardt, J. H. Engberg, T. K. Fischer and S. G. Lassen, *PLoS One*, 2014, **9**, e105053.
6 A. Abbott and H. Pearson, *Nature*, 2004, **427**, 472–473.
7 F. Karasek and O. Hutzinger, *Anal. Chem.*, 1986, **58**, 633A–642A.
8 A. J. Haes, C. L. Haynes, A. D. McFarland, G. C. Schatz, R. P. Van Duyne and S. Zou, *MRS Bull.*, 2005, **30**, 368–375.
9 A. J. Haes and R. P. Van Duyne, *Anal. Bioanal. Chem.*, 2004, **379**, 920–930.
10 S. Link and M. A. El-Sayed, *J. Phys. Chem. B*, 1999, **103**, 8410–8426.
11 B. Sepúlveda, P. C. Angelomé, L. M. Lechuga and L. M. Liz-Marzán, *Nano Today*, 2009, **4**, 244–251.
12 J. Mock, M. Barbic, D. Smith, D. Schultz and S. Schultz, *J. Chem. Phys.*, 2002, **116**, 6755–6759.
13 C. L. Haynes and R. P. Van Duyne, *J. Phys. Chem. B*, 2001, **105**, 5599–5611.
14 W. L. Daniel, M. S. Han, J.-S. Lee and C. A. Mirkin, *J. Am. Chem. Soc.*, 2009, **131**, 6362–6363.
15 F. Xia, X. Zuo, R. Yang, Y. Xiao, D. Kang, A. Vallée-Bélisle, X. Gong, J. D. Yuen, B. B. Hsu and A. J. Heeger, *Proc. Natl. Acad. Sci. U. S. A.*, 2010, **107**, 10837–10841.
16 J. Du, B. Zhu and X. Chen, *Small*, 2013, **9**, 4104–4111.
17 G. C. Schatz, M. A. Young and R. P. Van Duyne, *Surface-enhanced Raman Scattering*, Springer, 2006, pp. 19–45.
18 C. L. Haynes, A. D. McFarland and R. P. V. Duyne, *Anal. Chem.*, 2005, 77, 338 A–346 A.
19 S. Nie and S. R. Emory, *Science*, 1997, **275**, 1102–1106.
20 H. Liu, L. Zhang, X. Lang, Y. Yamaguchi, H. Iwasaki, Y. Inouye, Q. Xue and M. Chen, *Sci. Rep.*, 2011, **1**, 1–5.
21 J. Kneipp, H. Kneipp and K. Kneipp, *Chem. Soc. Rev.*, 2008, **37**, 1052–1060.
22 K. Kneipp, Y. Wang, H. Kneipp, L. T. Perelman, I. Itzkan, R. R. Dasari and M. S. Feld, *Phys. Rev. Lett.*, 1997, **78**, 1667.
23 E. Podstawka, Y. Ozaki and L. M. Proniewicz, *Appl. Spectrosc.*, 2005, **59**, 1516–1526.
24 J. C. Costa, R. A. Ando, P. H. Camargo and P. Corio, *J. Phys. Chem. C*, 2011, **115**, 4184–4190.
25 N. A. Abu Hatab, J. M. Oran and M. J. Sepaniak, *ACS Nano*, 2008, **2**, 377–385.
26 R. Tan, A. Agarwal, N. Balasubramanian, D. Kwong, Y. Jiang, E. Widjaja and M. Garland, *Sens. Actuators, A*, 2007, **139**, 36–41.
27 W. J. Cho, Y. Kim and J. K. Kim, *ACS Nano*, 2011, **6**, 249–255.
28 A. Campion and P. Kambhampati, *Chem. Soc. Rev.*, 1998, **27**, 241–250.
29 K. Kneipp, H. Kneipp, I. Itzkan, R. R. Dasari and M. S. Feld, *Chem. Rev.*, 1999, **99**, 2957–2976.
30 M. D. Porter, R. J. Lipert, L. M. Siperko, G. Wang and R. Narayanan, *Chem. Soc. Rev.*, 2008, **37**, 1001–1011.
31 Y. Wang, B. Yan and L. Chen, *Chem. Rev.*, 2012, **113**, 1391–1428.
32 M. Vendrell, K. K. Maiti, K. Dhaliwal and Y. T. Chang, *Trends Biotechnol.*, 2013, **31**, 249–257.
33 S. C. Luo, K. Sivashanmugan, J. D. Liao, C. K. Yao and H. C. Peng, *Biosens. Bioelectron.*, 2014, **61**, 232–240.
34 R. A. Halvorson and P. J. Vikesland, *Environ. Sci. Technol.*, 2010, **44**, 7749–7755.
35 B. Sharma, R. R. Frontiera, A. I. Henry, E. Ringe and R. P. Van Duyne, *Mater. Today*, 2012, **15**, 16–25.
36 S. Schlücker, *Angew. Chem., Int. Ed.*, 2014, **53**, 4756–4795.
37 D. Liu, Z. Wang and X. Jiang, *Nanoscale*, 2011, **3**, 1421–1433.
38 W. Zhao, M. A. Brook and Y. Li, *ChemBioChem*, 2008, **9**, 2363–2371.
39 D. Vilela, M. C. González and A. Escarpa, *Anal. Chim. Acta*, 2012, **751**, 24–43.
40 S. Su, W. Wu, J. Gao, J. Lu and C. Fan, *J. Mater. Chem.*, 2012, **22**, 18101–18110.
41 R. Alvarez-Puebla and L. Liz-Marzan, *Energy Environ. Sci.*, 2010, **3**, 1011–1017.
42 T. Masciangioli and W. X. Zhang, *Environ. Sci. Technol.*, 2003, **37**, 102A–108A.
43 C. Wang and C. Yu, *Rev. Anal. Chem.*, 2013, **32**, 1–14.
44 L. Wang, W. Ma, L. Xu, W. Chen, Y. Zhu, C. Xu and N. A. Kotov, *Mater. Sci. Eng., R*, 2010, **70**, 265–274.
45 P. J. Vikesland and K. R. Wigginton, *Environ. Sci. Technol.*, 2010, **44**, 3656–3669.
46 S. Szunerits and R. Boukherroub, *Chem. Commun.*, 2012, **48**, 8999–9010.
47 J. N. Anker, W. P. Hall, O. Lyandres, N. C. Shah, J. Zhao and R. P. Van Duyne, *Nat. Mater.*, 2008, **7**, 442–453.
48 J. Homola, *Chem. Rev.*, 2008, **108**, 462–493.
49 R. A. Alvarez-Puebla and L. M. Liz-Marzán, *Angew. Chem., Int. Ed.*, 2012, **51**, 11214–11223.
50 Y. Sun and Y. Xia, *Analyst*, 2003, **128**, 686–691.
51 P. Mulvaney, *Langmuir*, 1996, **12**, 788–800.
52 A. Zielińska, E. Skwarek, A. Zaleska, M. Gazda and J. Hupka, *Procedia Chem.*, 2009, **1**, 1560–1566.
53 S. Link and M. A. El-Sayed, *Annu. Rev. Phys. Chem.*, 2003, **54**, 331–366.
54 C. J. Orendorff, T. K. Sau and C. J. Murphy, *Small*, 2006, **2**, 636–639.
55 C. L. Nehl and J. H. Hafner, *J. Mater. Chem.*, 2008, **18**, 2415–2419.
56 L. Zhong, X. Zhou, S. Bao, Y. Shi, Y. Wang, S. Hong, Y. Huang, X. Wang, Z. Xie and Q. Zhang, *J. Mater. Chem.*, 2011, **21**, 14448–14455.
57 I. Blakey, Z. Merican and K. J. Thurecht, *Langmuir*, 2013, **29**, 8266–8274.
58 K. A. Willets and R. P. Van Duyne, *Annu. Rev. Phys. Chem.*, 2007, **58**, 267–297.
59 J. J. Storhoff, R. Elghanian, R. C. Mucic, C. A. Mirkin and R. L. Letsinger, *J. Am. Chem. Soc.*, 1998, **120**, 1959–1964.
60 C. C. Huang and H. T. Chang, *Chem. Commun.*, 2007, 1215–1217.

61 J. Liu and Y. Lu, *Angew. Chem.*, 2006, **118**, 96–100.
62 I. Mrozek and A. Otto, *J. Electron Spectrosc. Relat. Phenom.*, 1990, **54**, 895–911.
63 G. Compagnini, C. Galati and S. Pignataro, *Phys. Chem. Chem. Phys.*, 1999, **1**, 2351–2353.
64 K. H. Su, Q. H. Wei, X. Zhang, J. Mock, D. R. Smith and S. Schultz, *Nano Lett.*, 2003, **3**, 1087–1090.
65 X. Qian, X. Zhou and S. Nie, *J. Am. Chem. Soc.*, 2008, **130**, 14934–14935.
66 L. Qin, S. Zou, C. Xue, A. Atkinson, G. C. Schatz and C. A. Mirkin, *Proc. Natl. Acad. Sci. U. S. A.*, 2006, **103**, 13300–13303.
67 H. Im, K. C. Bantz, N. C. Lindquist, C. L. Haynes and S. H. Oh, *Nano Lett.*, 2010, **10**, 2231–2236.
68 H. Wang, C. S. Levin and N. J. Halas, *J. Am. Chem. Soc.*, 2005, **127**, 14992–14993.
69 K. L. Wustholz, A.-I. Henry, J. M. McMahon, R. G. Freeman, N. Valley, M. E. Piotti, M. J. Natan, G. C. Schatz and R. P. V. Duyne, *J. Am. Chem. Soc.*, 2010, **132**, 10903–10910.
70 L. Fabris, A. S. D. Indrasekara, S. Meyers, S. Shubeita, L. C. Feldman and T. Gustafsson, *Nanoscale*, 2014.
71 M. Potara, A. M. Gabudean and S. Astilean, *J. Mater. Chem.*, 2011, **21**, 3625–3633.
72 A. McLintock, C. A. Cunha-Matos, M. Zagnoni, O. R. Millington and A. W. Wark, *ACS Nano*, 2014, **8**, 8600–8609.
73 G. Braun, I. Pavel, A. R. Morrill, D. S. Seferos, G. C. Bazan, N. O. Reich and M. Moskovits, *J. Am. Chem. Soc.*, 2007, **129**, 7760–7761.
74 S. L. Kleinman, R. R. Frontiera, A.-I. Henry, J. A. Dieringer and R. P. Van Duyne, *Phys. Chem. Chem. Phys.*, 2013, **15**, 21–36.
75 A. Shiohara, Y. Wang and L. M. Liz-Marzán, *J. Photochem. Photobiol., C*, 2014, **21**, 2–25.
76 N. H. Kim, S. J. Lee and M. Moskovits, *Adv. Mater.*, 2011, **23**, 4152–4156.
77 R. A. Alvarez-Puebla, E. Arceo, P. J. Goulet, J. J. Garrido and R. F. Aroca, *J. Phys. Chem. B*, 2005, **109**, 3787–3792.
78 L. S. Lawson, J. W. Chan and T. Huser, *Nanoscale*, 2014, **6**, 7971–7980.
79 K. V. Kong, U. Dinish, W. K. O. Lau and M. Olivo, *Biosens. Bioelectron.*, 2014, **54**, 135–140.
80 W. Ji, N. Spegazzini, Y. Kitahama, Y. Chen, B. Zhao and Y. Ozaki, *J. Phys. Chem. Lett.*, 2012, **3**, 3204–3209.
81 W. Hill and B. Wehling, *J. Phys. Chem.*, 1993, **97**, 9451–9455.
82 R. Alvarez-Puebla, B. Cui, J. P. Bravo-Vasquez, T. Veres and H. Fenniri, *J. Phys. Chem. C*, 2007, **111**, 6720–6723.
83 U. K. Sarkar, *Chem. Phys. Lett.*, 2003, **374**, 341–347.
84 H. Yuan, A. M. Fales, C. G. Khoury, J. Liu and T. Vo-Dinh, *J. Raman Spectrosc.*, 2013, **44**, 234–239.
85 D. K. Lim, I. J. Kim and J. M. Nam, *Chem. Commun.*, 2008, 5312–5314.
86 C. J. Murphy, T. K. Sau, A. M. Gole, C. J. Orendorff, J. Gao, L. Gou, S. E. Hunyadi and T. Li, *J. Phys. Chem. B*, 2005, **109**, 13857–13870.
87 L. J. Sherry, R. Jin, C. A. Mirkin, G. C. Schatz and R. P. Van Duyne, *Nano Lett.*, 2006, **6**, 2060–2065.
88 J. E. Millstone, S. Park, K. L. Shuford, L. Qin, G. C. Schatz and C. A. Mirkin, *J. Am. Chem. Soc.*, 2005, **127**, 5312–5313.
89 L. Rodríguez-Lorenzo, R. A. Alvarez-Puebla, I. Pastoriza-Santos, S. Mazzucco, O. Stéphan, M. Kociak, L. M. Liz-Marzán and F. J. García de Abajo, *J. Am. Chem. Soc.*, 2009, **131**, 4616–4618.
90 C. J. Orendorff, L. Gearheart, N. R. Jana and C. J. Murphy, *Phys. Chem. Chem. Phys.*, 2006, **8**, 165–170.
91 S. E. Bell and M. R. McCourt, *Phys. Chem. Chem. Phys.*, 2009, **11**, 7455–7462.
92 T. Iliescu, M. Baia and W. Kiefer, *Chem. Phys.*, 2004, **298**, 167–174.
93 H. Y. Lin, C. H. Huang, W. H. Hsieh, L. H. Liu, Y. C. Lin, C. C. Chu, S. T. Wang, I. Kuo, L. K. Chau and C. Y. Yang, *Small*, 2014, **10**, 4700–4710.
94 C. A. Mirkin, R. L. Letsinger, R. C. Mucic and J. J. Storhoff, *Nature*, 1996, **382**, 607–609.
95 R. A. Reynolds, C. A. Mirkin and R. L. Letsinger, *J. Am. Chem. Soc.*, 2000, **122**, 3795–3796.
96 D. G. Thompson, A. Enright, K. Faulds, W. E. Smith and D. Graham, *Anal. Chem.*, 2008, **80**, 2805–2810.
97 L. Liu, S. Li, L. Liu, D. Deng and N. Xia, *Analyst*, 2012, **137**, 3794–3799.
98 D. E. Huizenga and J. W. Szostak, *Biochemistry*, 1995, **34**, 656–665.
99 J. Liu and Y. Lu, *Nat. Protoc.*, 2006, **1**, 246–252.
100 Z. Zhu, C. Wu, H. Liu, Y. Zou, X. Zhang, H. Kang, C. J. Yang and W. Tan, *Angew. Chem.*, 2010, **122**, 1070–1074.
101 A. Sugunan, C. Thanachayanont, J. Dutta and J. Hilborn, *Sci. Technol. Adv. Mater.*, 2005, **6**, 335–340.
102 J. Liu and Y. Lu, *J. Am. Chem. Soc.*, 2003, **125**, 6642–6643.
103 C. Y. Lin, C. J. Yu, Y. H. Lin and W. L. Tseng, *Anal. Chem.*, 2010, **82**, 6830–6837.
104 A. E. Üzer, Z. Can, I. l. Akın, E. Erçağ and R. A. Apak, *Anal. Chem.*, 2013, **86**, 351–356.
105 F. M. Li, J. M. Liu, X. X. Wang, L. P. Lin, W. L. Cai, X. Lin, Y. N. Zeng, Z. M. Li and S. Q. Lin, *Sens. Actuators, B*, 2011, **155**, 817–822.
106 Z. Zhang, Z. Chen, C. Qu and L. Chen, *Langmuir*, 2014, **30**, 3625–3630.
107 G. Wang, Z. Chen, W. Wang, B. Yan and L. Chen, *Analyst*, 2011, **136**, 174–178.
108 W. Zhao, M. M. Ali, S. D. Aguirre, M. A. Brook and Y. Li, *Anal. Chem.*, 2008, **80**, 8431–8437.
109 S. C. Tseng, C. C. Yu, D. Wan, H. L. Chen, L. A. Wang, M. C. Wu, W. F. Su, H. C. Han and L. C. Chen, *Anal. Chem.*, 2012, **84**, 5140–5145.
110 D. Mazumdar, J. Liu, G. Lu, J. Zhou and Y. Lu, *Chem. Commun.*, 2010, **46**, 1416–1418.
111 N. Ratnarathorn, O. Chailapakul, C. S. Henry and W. Dungchai, *Talanta*, 2012, **99**, 552–557.
112 M. Fleischmann, P. Hendra and A. McQuillan, *Chem. Phys. Lett.*, 1974, **26**, 163–166.
113 T. Vo-Dinh, M. Hiromoto, G. Begun and R. Moody, *Anal. Chem.*, 1984, **56**, 1667–1670.

114 M. M. Carrabba, R. B. Edmonds and R. D. Rauh, *Anal. Chem.*, 1987, **59**, 2559–2563.
115 R. W. Taylor, R. J. Coulston, F. Biedermann, S. Mahajan, J. J. Baumberg and O. A. Scherman, *Nano Lett.*, 2013, **13**, 5985–5990.
116 D. K. Lim, K. S. Jeon, J. H. Hwang, H. Kim, S. Kwon, Y. D. Suh and J. M. Nam, *Nat. Nanotechnol.*, 2011, **6**, 452–460.
117 B. Saute, R. Premasiri, L. Ziegler and R. Narayanan, *Analyst*, 2012, **137**, 5082–5087.
118 D. K. Lim, K. S. Jeon, H. M. Kim, J. M. Nam and Y. D. Suh, *Nat. Mater.*, 2009, **9**, 60–67.
119 J. Yang, M. Palla, F. G. Bosco, T. Rindzevicius, T. S. Alstrøm, M. S. Schmidt, A. Boisen, J. Ju and Q. Lin, *ACS Nano*, 2013, **7**, 5350–5359.
120 W. Leng and P. J. Vikesland, *Langmuir*, 2014, **30**, 8342–8349.
121 S. Basu, S. Pande, S. Jana, S. Bolisetty and T. Pal, *Langmuir*, 2008, **24**, 5562–5568.
122 R. W. Taylor, T. C. Lee, O. A. Scherman, R. Esteban, J. Aizpurua, F. M. Huang, J. J. Baumberg and S. Mahajan, *ACS Nano*, 2011, **5**, 3878–3887.
123 L. Zhang, X. Lang, A. Hirata and M. Chen, *ACS Nano*, 2011, **5**, 4407–4413.
124 A. Tao, F. Kim, C. Hess, J. Goldberger, R. He, Y. Sun, Y. Xia and P. Yang, *Nano Lett.*, 2003, **3**, 1229–1233.
125 T. H. Reilly, J. D. Corbman and K. L. Rowlen, *Anal. Chem.*, 2007, **79**, 5078–5081.
126 Y. Jin, *Adv. Mater.*, 2012, **24**, 5153–5165.
127 P. Wang, O. Liang, W. Zhang, T. Schroeder and Y. H. Xie, *Adv. Mater.*, 2013, **25**, 4918–4924.
128 R. Zhang, B. B. Xu, X. Q. Liu, Y. L. Zhang, Y. Xu, Q. D. Chen and H. B. Sun, *Chem. Commun.*, 2012, **48**, 5913–5915.
129 C. H. Lee, L. Tian and S. Singamaneni, *ACS Appl. Mater. Interfaces*, 2010, **2**, 3429–3435.
130 W. Zhang, B. Li, L. Chen, Y. Wang, D. Gao, X. Ma and A. Wu, *Anal. Methods*, 2014, **6**, 2066–2071.
131 Y. H. Ngo, D. Li, G. P. Simon and G. Garnier, *Langmuir*, 2012, **28**, 8782–8790.
132 L. Polavarapu and L. M. Liz-Marzán, *Phys. Chem. Chem. Phys.*, 2013, **15**, 5288–5300.
133 A. Abbas, A. Brimer, J. M. Slocik, L. Tian, R. R. Naik and S. Singamaneni, *Anal. Chem.*, 2013, **85**, 3977–3983.
134 L. Zhang, X. Gong, Y. Bao, Y. Zhao, M. Xi, C. Jiang and H. Fong, *Langmuir*, 2012, **28**, 14433–14440.
135 D. He, B. Hu, Q. F. Yao, K. Wang and S. H. Yu, *ACS Nano*, 2009, **3**, 3993–4002.
136 H. Ko, S. Chang and V. V. Tsukruk, *ACS Nano*, 2008, **3**, 181–188.
137 P. Aldeanueva-Potel, E. Faoucher, R. N. A. Alvarez-Puebla, L. M. Liz-Marzán and M. Brust, *Anal. Chem.*, 2009, **81**, 9233–9238.
138 X. Zhou, F. Zhou, H. Liu, L. Yang and J. Liu, *Analyst*, 2013, **138**, 5832–5838.
139 B. Saute and R. Narayanan, *Analyst*, 2011, **136**, 527–532.
140 S. Abalde-Cela, S. Ho, B. Rodríguez-González, M. A. Correa-Duarte, R. A. Álvarez-Puebla, L. M. Liz-Marzán and N. A. Kotov, *Angew. Chem.*, 2009, **121**, 5430–5433.
141 S. S. Dasary, A. K. Singh, D. Senapati, H. Yu and P. C. Ray, *J. Am. Chem. Soc.*, 2009, **131**, 13806–13812.
142 L. Guerrini, J. V. Garcia-Ramos, C. Domingo and S. Sanchez-Cortes, *Anal. Chem.*, 2009, **81**, 953–960.
143 R. A. Álvarez-Puebla, R. Contreras-Cáceres, I. Pastoriza-Santos, J. Pérez-Juste and L. M. Liz-Marzán, *Angew. Chem., Int. Ed.*, 2009, **48**, 138–143.
144 L. Guerrini, J. V. Garcia-Ramos, C. Domingo and S. Sanchez-Cortes, *Anal. Chem.*, 2009, **81**, 1418–1425.
145 P. Leyton, C. Domingo, S. Sanchez-Cortes, M. Campos-Vallette and J. Garcia-Ramos, *Langmuir*, 2005, **21**, 11814–11820.
146 L. Guerrini, J. V. Garcia-Ramos, C. Domingo and S. Sanchez-Cortes, *Langmuir*, 2006, **22**, 10924–10926.
147 S. Z. Nergiz, N. Gandra, M. E. Farrell, L. Tian, P. M. Pellegrino and S. Singamaneni, *J. Mater. Chem. A*, 2013, **1**, 6543–6549.
148 A. Kolomijeca, Y. Kwon, K. Sowoidnich, R. Prien, D. Schulz-Bull and H. Kronfeldt, *Proc. 21th*, 2011, 859862.
149 H. Schmidt, N. Bich Ha, J. Pfannkuche, H. Amann, H.-D. Kronfeldt and G. Kowalewska, *Mar. Pollut. Bull.*, 2004, **49**, 229–234.
150 J. Pfannkuche, L. Lubecki, H. Schmidt, G. Kowalewska and H.-D. Kronfeldt, *Mar. Pollut. Bull.*, 2012, **64**, 614–626.
151 R. J. Rubira, S. A. Camacho, P. H. Aoki, M. D. Maximino, P. Alessio, C. S. Martin, O. N. Oliveira Jr, F. M. Fatore, F. V. Paulovich and C. J. Constantino, *Colloid Polym. Sci.*, 2014, **1–10**.
152 J. Zheng, S. Pang, T. P. Labuza and L. He, *Analyst*, 2013, **138**, 7075–7078.
153 L. XuanáQuang, G. HunáSeong and K. JunáDo, *Lab Chip*, 2008, **8**, 2214–2219.
154 D. Lin, T. Qin, Y. Wang, X. Sun and L. Chen, *ACS Appl. Mater. Interfaces*, 2014, **6**, 1320–1329.
155 K. L. Rule and P. J. Vikesland, *Environ. Sci. Technol.*, 2009, **43**, 1147–1152.
156 K. K. Maiti, U. Dinish, C. Y. Fu, J. J. Lee, K. S. Soh, S. W. Yun, R. Bhuvaneswari, M. Olivo and Y. T. Chang, *Biosens. Bioelectron.*, 2010, **26**, 398–403.
157 B. Guven, N. Basaran-Akgul, E. Temur, U. Tamer and İ. H. Boyacı, *Analyst*, 2011, **136**, 740–748.
158 S. Deng, W. Xu, J. Wang, X. Ling, J. Wu, L. Xie, J. Kong, M. S. Dresselhaus and J. Zhang, *Nano Res.*, 2014, **7**, 1271–1279.
159 R. A. Tripp, R. A. Dluhy and Y. Zhao, *Nano Today*, 2008, **3**, 31–37.